Pulmonary Blood Flow Increases in Damaged Regions Directly after Acid Aspiration in Rats

Torsten Richter, M.D.,* Ralf Bergmann, Ph.D.,† Lilla Knels, M.D.,‡ Frank Hofheinz, Ph.D.,† Michael Kasper, Ph.D.,§ Martin Deile, M.D.,* Jens Pietzsch, Ph.D.,‖ Maximilian Ragaller, M.D.,# Thea Koch, M.D.**

ABSTRACT

Background: After gastric aspiration events, patients are at risk of pulmonary dysfunction and the development of severe acute lung injury and acute respiratory distress syndrome, which may contribute to the development of an inflammatory reaction. The authors' aim in the current study was to investigate the role of the spatial distribution of pulmonary blood flow in the pathogenesis of pulmonary dysfunction during the early stages after acid aspiration.

Methods: The authors analyzed the pulmonary distribution of radiolabeled microspheres in normal (n = 6) and injured (n = 12) anesthetized rat lungs using positron emission tomography, computed tomography, and histological examination.

Results: Injured regions demonstrate increased pulmonary blood flow in association with reduced arterial pressure and the deterioration of arterial oxygenation. After acid aspiration, computed tomography scans revealed that lung density had increased in the injured regions and that these regions colocalized with areas of increased blood flow. The acid was instilled into the middle and basal regions of the lungs. The blood flow was significantly increased to these regions compared with the blood flow to uninjured lungs in the control animals (middle region: 1.23 [1.1; 1.4] (median [25%; 75%]) *vs.* 1.04 [1.0; 1.1] and basal region: 1.25 [1.2; 1.3] *vs.* 1.02 [1.0; 1.05], respectively). The increase in blood flow did not seem to be due to vascular leakage into these injured areas.

Conclusions: The data suggest that 10 min after acid aspiration, damaged areas are characterized by increased pulmonary blood flow. The results may impact further treatment strategies, such as drug targeting.

What We Already Know About This Topic

- Acute lung injury is a recognized complication of gastric aspiration, which can cause histological damage
- Hyperperfusion can be associated with alveolar damage

What This Article Tells Us That Is New

- In the early stage of inflammation after acid-induced acute lung injury, the pulmonary blood flow is distributed heterogeneously
- Areas of aspiration damage are congruent with regions of higher blood flow 10 min after injury

ACID aspiration is a major cause of acute lung injury (ALI) and acute respiratory distress syndrome.[1,2] Approximately 15–16.5% of patients with acid aspiration may develop ALI,[3,4] and the incidence increases with further predisposing conditions (*e.g.*, sepsis or trauma) and risk factors (*e.g.*, chemotherapy or obesity).[5] The type of aspirate can vary from fluid content (liquid, blood, or secretions) to food particles. Aspiration can cause an initial episode of pneumonitis, which may be complicated by subsequent bacterial pneumonia.[5] ALI pneumonitis secondary to aspiration carries a mortality rate of 44%.[6]

The induction of pulmonary leukocyte sequestration and the disruption of capillary–alveolar barrier function were shown to be responsible for the development of pulmonary edema in animal models of acid-induced ALI.[7–10] In addition, polymorphonuclear leukocyte migration is initiated *via* diapedesis through the alveolar capillaries in response to

* Staff Anesthetist, # Professor and Head of the Intensive Care Unit, ** Professor and Chair of the Department, Department of Anesthesia and Intensive Care, Carl Gustav Carus University Hospital, University of Technology, Dresden, Germany. † Senior Scientist, ‖ Professor, Head of the Division of Radiopharmaceutical Biology, Institute of Radiopharmacy, Helmholtz-Zentrum Dresden-Rossendorf, Dresden, Germany. ‡ Senior Scientist, § Professor, Head of the Institute of Anatomy, University of Technology.

Received from Helmholtz-Zentrum Dresden-Rossendorf, Dresden, Germany. Submitted for publication April 3, 2012. Accepted for publication June 12, 2013. Support was provided solely from institutional and/or departmental sources. The authors declare no competing interests. Drs. Richter and Bergmann contributed equally to this work.

Address correspondence to Dr. Richter: Department of Anesthesia and Intensive Care, University Hospital, TU Dresden, Fetscherstrasse 74, 01307 Dresden, Germany. torsten.richter@uniklinikum-dresden.de. Anesthesiology 2013; 119:890-900

◆ This article is accompanied by an Editorial View. Please see: Miller DW, Pittet J-F: Targeting aspiration pneumonitis. ANESTHESIOLOGY 2013; 119:752–4.

Supplemental digital content is available for this article. Direct URL citations appear in the printed text and are available in both the HTML and PDF versions of this article. Links to the digital files are provided in the HTML text of this article on the Journal's Web site (www.anesthesiology.org).

inflammation.[11] Although aspiration injury has been investigated extensively, its impact on spatial pulmonary blood flow (PBF) during the early phase of injury has not been carefully evaluated. Data regarding very early pathophysiological changes are highly desirable, as the clinician must react within minutes after an aspiration event.

Experimental interventions that have been suggested to treat acid-induced lung damage include intravenous hyperosmolar solutions,[7] hypertonic saline solutions,[12] and pentoxifylline.[13] Studying the regional blood flow pattern after an aspiration event could contribute to the development of novel therapeutic approaches, such as drug targeting. In the current study, we characterize the spatial PBF shortly after acid aspiration using radiolabeled microspheres and positron emission tomography (PET). A preliminary analysis of portions of this study has been previously reported in abstract form.[14]

Material and Methods

Experimental Procedures

After receiving approval from the local Animal Care Committee (Landesdirektion Dresden, Saxony, Germany), 18 male Wistar-Unilever rats (293–500 g) were included in this study. We anesthetized the rats using a combination of desflurane (7–12%), a single intraperitoneal injection of ketamine (75 mg/kg), and 1% lignocain infiltrated into the operative field. Catheters were introduced into the femoral artery (0.9-mm Leader catheter; Vygon, Ecouen, France) and femoral vein (0.8-mm Umbilical Vessel Catheter; Tyco Healthcare, Tullamore, Ireland) to measure arterial blood pressure and heart rate (Component Monitoring System; Hewlett-Packard Model 54S; Saronno, Italy), to obtain arterial blood samples for the blood gas analyses (ABL 50; Radiometer, Copenhagen, Denmark), to measure hematocrit, and to provide intravenous infusions. The spontaneously breathing animals were allowed to stabilize for 30 min after preparation and were then randomly assigned to either the control (n = 6) or the injury group (n = 12).

ALI was induced *via* the instillation of 0.1 M HCl (0.4 ml/kg body weight) through a tracheostomy tube with a catheter inserted to maximum depth, causing selective injury to either the left or right lung at random. The control group received no treatment through the catheter.

We measured physiologic parameters (blood gases and hemodynamics) at baseline and 10 min after the infusion of the radiolabeled microspheres. Human serum albumin microspheres with a mean diameter of 20 μm were labeled with Gallium-68 (^{68}Ga), as previously described,[15] which yielded injectable ^{68}Ga human serum albumin microspheres (Ga-68 microspheres).

Positron Emission Tomography Imaging. Spatial PBF was determined using a small animal PET scanner (microPET® P4; Siemens Preclinical Solutions, Knoxville, TN). After a 10-min transmission scan, a 1-min bolus infusion of Ga-68 microspheres was initiated, and then a 30-min emission scan was performed. In 6 of the 12 injured animals, we performed a second transmission scan immediately after the 30-min emission scan to measure the potential influence of local density changes on the PET volume data and calculate altered PBF after injury. PBF differences between the left and right lobe were compared using different attenuation corrections (determined by transmission before and after the emission scan). The emission scans were corrected for decay and attenuation, and the frames were reconstructed using Ordered Subset Expectation Maximization that was applied to 3D sinograms with 14 subsets, six Ordered Subset Expectation Maximization 3D iterations, two maximum a posteriori iterations, and a 0.05 β-value for smoothing.

Computer Tomography Imaging. The degree of injury was assessed through lung density measurements, which were obtained from 10-min computer tomography (CT) scans of the entire lung acquired at baseline and at the end of the experiment using a micro-CT scanner (SkyScan 1178 micro-CT system; SkyScan, Kontich, Belgium) with the following specifications: 360 degrees of scanning, averaging two frames; 83-μm pixels; 85-mm field of view, scanning time of 9 min and 7 s; and a voltage of 65 kV and 615 μA. After the final measurement, the animals were sacrificed, and the lungs were extracted for postmortem analysis (fig. 1).

Postmortem Analysis. The lungs were removed at continuous airway pressures equal to an intrabronchial pressure of 7 cm H_2O and preserved for microsphere and tissue analyses. After extraction, the lungs were immediately frozen at −50°C using isopentane/dry ice and stored at −64°C. Six specimens were removed, embedded in tissue-freezing medium (Jung; Leica Microsystems, Wetzlar, Germany), and cut into 20-μm slices of the entire transverse plane (apical: 0.5 cm below the upper apex; middle: at the tracheal bifurcation level; basal: 1 cm above the most basal lung tissue) using a microtome (Leica CM 3000 cryostat, Leica Microsystems) at −20°C. Microscopic photographs were taken (AxioImager.A1) and processed (Axiovision, AxioVs40 V4.8.1.0; Carl Zeiss Imaging Solutions, Jena, Germany). After the addition of the mosaic pictures, complete images of the selected lung layer were obtained. The entire representative transverse planes of the apical, middle, and basal lung tissues were analyzed to determine the concentration of microspheres present. Diffuse alveolar damage (DAD) was evaluated by an expert blinded to the protocol using a weighted histological score.[16] Values from 0 to 3 (0 = normal; 1 = slight effect; 2 = intermediate effect; and 3 = severe effect) represent the severity of each feature (alveolar edema, interstitial edema, microhemorrhage, inflammatory infiltration of polymorphonuclear neutrophils and macrophages, microatelectasis, and alveolar overdistension). The extent of damage in each sector was recorded as follows: 0 = no damage; 1 = up to 25% damage; 2 = 25–50% damage; 3 = 50–75% damage; 4 = 75% to approximately complete damage; and 5 = complete damage. When multiplied, the severity of the feature and the extent of damage produced values between 0 and 15, which were averaged for each region. Finally, we performed scanning

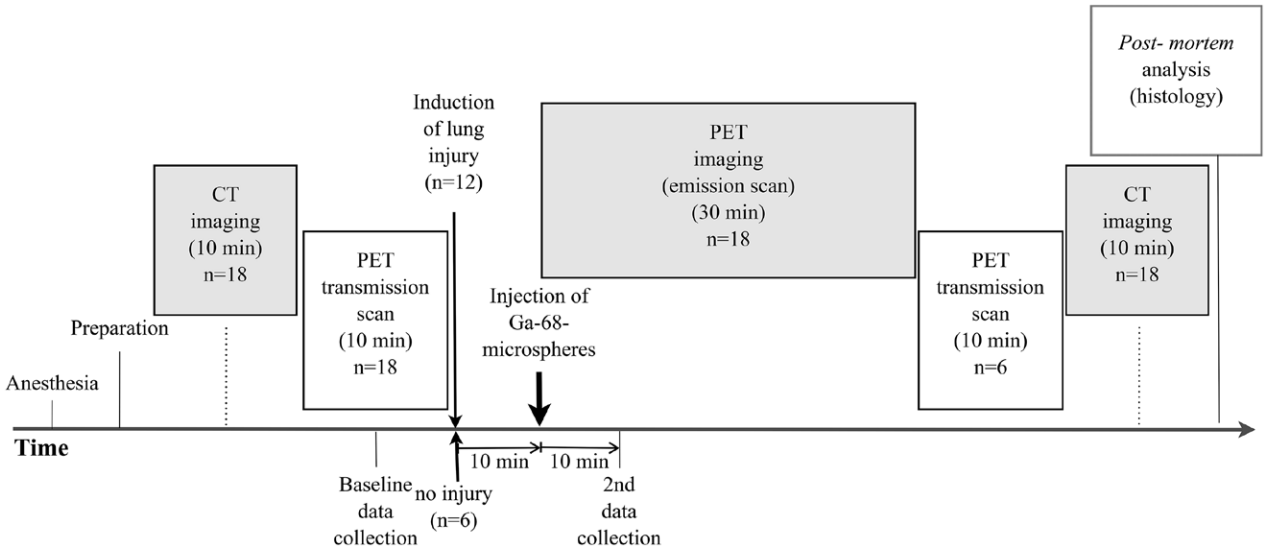

Fig. 1. Study protocol scheme. CT = computer tomography; PET = positron emission tomography.

electron microscopy (LEO S430; Carl Zeiss, Oberkochen, Germany) on representative lung specimens.

Image Processing. Computer tomography scans were coregistered to the PET scans, and regions of interest (ROI) were defined (fig. 2). PBF was calculated by analyzing the pulmonary distribution of Ga-68 microspheres within the ROIs (right and left lungs, $ROI_{specific}$).[15] $ROI_{specific}$ was defined by placing a spherical ROI of 0.24 cm^3 over the area with the greatest Ga-68 microsphere concentration. An identical $ROI_{specific}$ of the same volume was then placed on the contralateral lung in an anatomically corresponding position (fig. 2) and layered over the coregistered second CT scan of the animal to assess lung density and to further calculate the correlation between PBF and lung density within this ROI. PBF for the entire lung and for $ROI_{specific}$ was analyzed as a ratio of right to left side for the control animals and for the injury to uninjured side for the aspiration group.

The standardized uptake value is defined as the Gallium-68 microspheres uptake in the selected lung regions (apical, medial, and basal ROIs for both groups) scaled by the administered activity and by the body weight of the rats studied, and the values were decay corrected with respect to the Gallium-68 half-life. To minimize recovery effects, we used maximal Gallium-68 microspheres uptake values to calculate maximal standardized uptake value.

Statistics

All data are presented as the medians values 25th and 75th percentiles (median [25%; 75%]), unless otherwise specified. A nonparametric Wilcoxon two-tailed, matched-pairs signed-rank test was used for data comparison within groups, and an two-tailed, unpaired *t* test with Welch correction was used when appropriate (GraphPad Prism 5.02 for Windows; GraphPad Software Inc., San Diego, CA). Statistical significance was assigned for *P* values less than 0.05.

Results

Global Physiologic Variables

Animals from the control and aspiration groups (weighing 340 g [313; 381] and 354 g [333; 460], respectively) did not differ in terms of the physiological values (table 1) recorded at baseline. Acid aspiration generated major changes in the injury group, including deterioration of blood gases and significantly reduced arterial pressure (table 1). Although arterial oxygen tension, arterial pH, and arterial oxygen saturation declined in the injury group, the arterial carbon dioxide tension, heart rate, and respiratory rate remained unaffected. The physiological variables for animals in the control group were stable, with no evidence of blood loss or changes in body temperature during the experiment. Separate analysis of gas exchange and respiratory rate, heart rate, and mean arterial pressure revealed no differences within the injury group between the left- and right-side injured animals.

Regional PBF

The PBF data are represented for different regions: right lung, left lung, $ROI_{specific}$ of the injured and uninjured lung and for three transversal planes (apical, middle, and basal) of each lung.

PBF in the Right Lung, Left Lung, and $ROI_{specific}$. PBF ratio of the right to the left lung for the control group was not significant different from the PBF ratio of the injured to the uninjured lung for the injury group (fig 3; $P = 0.16$). The PBF ratio of $ROI_{specific}$ of the injured to uninjured side was 1.2 (1.1;1.3). This PBF ratio for $ROI_{specific}$ was significantly higher in the injury group than the PBF ratio for $ROI_{specific}$ of right to left lung of the control group (fig. 3; $P < 0.0001$). This was a result of a higher PBF on the injured side (0.33 [0.29; 0.34]) compared with the uninjured side (0.26 [0.29; 0.34]; $P = 0.001$).

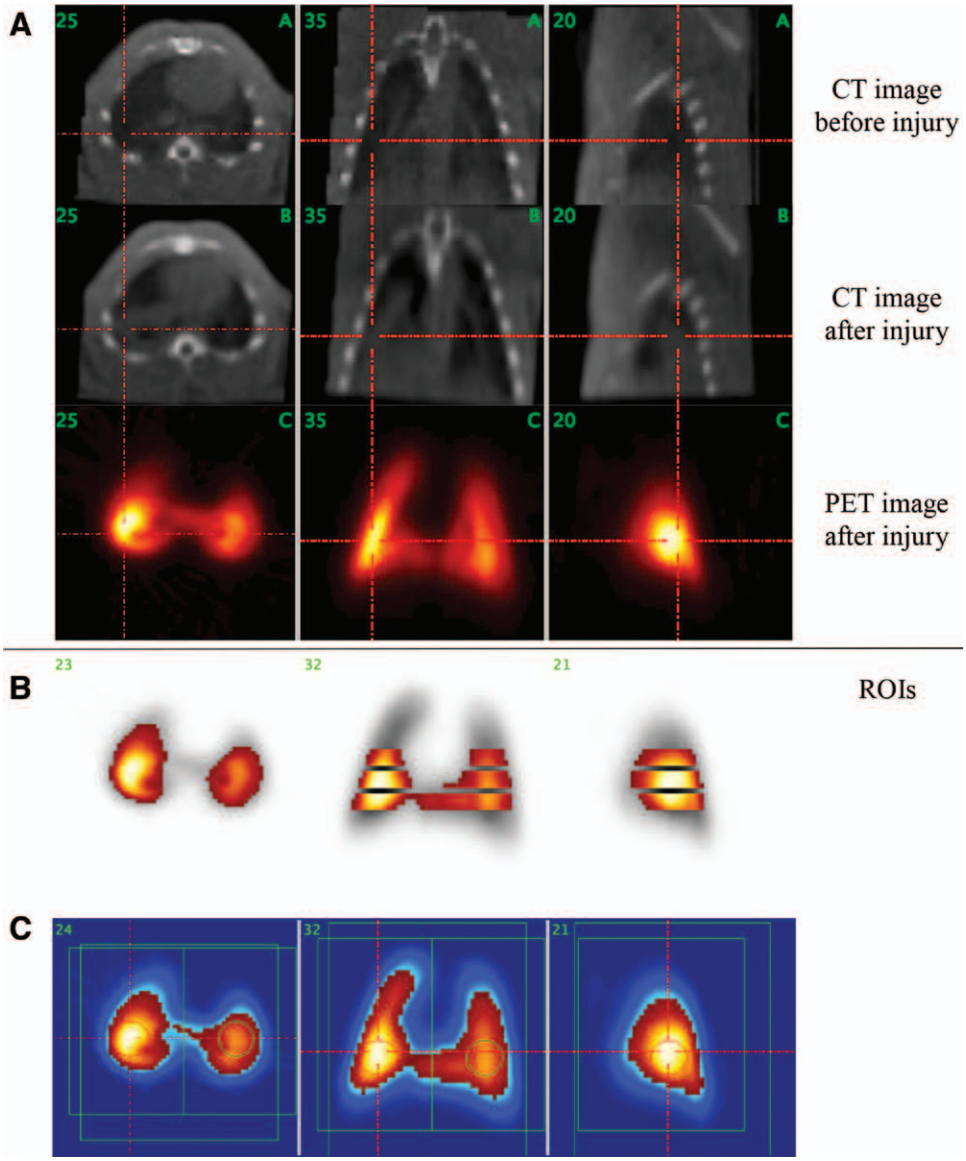

Fig. 2. Example of coregistered computer tomography (CT) and positron emission tomography (PET) images in the transverse, coronary, and sagittal planes. (*A*) *Red lines* are focused on the same area within the lung before and after injury in the CT and PET scans. *Dark areas* in the CT scan represent aerated zones. *Areas with high density* were formed in the right lung in the CT image after injury. *Color coding* shows a relative scale in which the measurements are normalized to their mean values and represent regional tracer concentrations of Ga-68 microspheres from high (*white*) to low (*black*), as determined by PET in MBq/cm^3. Higher concentrations of Ga-68 microspheres in the PET scan correspond to areas of higher density in the CT scan after injury. (*B*) Example of image processing after coregistration. Region of interest (ROI) definition: six ROIs (apical, medial, and caudal) used for the calculation of maximal standardized uptake value for each side of the lung. (*C*) *Rectangles* are ROI masks for the entire lung (ROI_{total}) and the right and left lungs in a three-dimensional environment. Areas with the greatest Ga-68 microsphere concentration were marked with a spherical ROI ([$ROI_{specific}$], 0.24 cm^3) on one lung. The contralateral $ROI_{specific}$ of the identical size was placed on the opposite lung in an anatomically corresponding position. Spherical ROIs ($ROI_{specific}$) were used for the calculation of PBF and to determine the correlation between CT and PET measurements. For all of the images from one animal, the same ROI masks were used for the threshold analysis with the PET and CT scans.

The distribution of the regional PBF was not different within the control group, when comparing PBF data from the left and the right lungs. The group that had acid instilled into the right lung had no statistically significant increase in PBF to the entire right lung. However, there was a statistically significant increase in PBF to the left-acid instilled lungs. The PBF for $ROI_{specific}$ was significantly higher in the injured lungs (table 2).

PBF in Apical, Middle, and Basal ROIs. The PBF ratio of right to left lung for the control group was significantly different from the PBF ratio of injured to uninjured lung in the injury group for all chosen ROIs (fig. 4). Moreover,

Table 1. Physiologic Variables

	Control		Injury	
	Baseline	After Injection of Ga-68 Microspheres	Baseline	After Injection of Ga-68 Microspheres
Pao_2, mmHg	108 [100; 121]	105 [89; 113]	123 [109; 139]	62 [59; 80]*
$Paco_2$, mmHg	52 [48; 55]	49 [47; 53]	55 [46; 56]	55 [48; 59]
pH	7.36 [7.3; 7.39]	7.36 [7.31; 7.39]	7.31 [7.26; 7.34]	7.28 [7.20; 7.32]*
$Spao_2$, %	97 [97; 98]	97 [96; 98]	98 [97; 99]	89 [84; 94]*
HR, beats/min	311 [263; 324]	301 [279; 332]	317 [288; 339]	308 [290; 329]
MAP, mmHg	80 [75; 85]	76 [74; 93]	88 [74; 104]	77 [68; 88]*
RR, beats/min	61 [60; 64]	60 [59; 66]	64 [60; 71]	65 [62; 70]
T, °C	36.3 [36; 36.9]	36.7 [36.4; 36.9]	36.3 [36; 36.9]	36.5 [36.2; 37.1]
Hct	0.44 [0.42; 0.47]	0.42 [0,41; 0,44]	0.44 [0.42; 0.48]	0.44 [0.41; 0.45]

Values represent the median values [interquartile range]; control n = 6; injury n = 12. Physiologic variables for measurements taken before and 10 min after the injection of Ga-68 microspheres; the second value in the injury group corresponds to values obtained 20 min after acid aspiration.

*$P < 0.01$.

Hct = hematocrit; HR = heart rate; MAP = mean arterial blood pressure; $Paco_2$ = arterial carbon dioxide tension; Pao_2 = arterial oxygen tension; pH = arterial pH; RR = respiration rate; $Spao_2$ = arterial oxygen saturation; T = body temperature.

the difference between the ratios appeared to progress from the apical to the basal regions, indicating a slightly increased blood flow along the cranial to caudal axis in injured regions. Animals that underwent acid aspiration showed higher ipsilateral maximal standardized uptake values for the injured side compared with the contralateral side (for all regions in the right injury group and the middle and basal ROIs in the group with left injuries). Left lung-injured animals demonstrated significant differences in PBF on both lungs compared with the control group, whereas an injury on the right lung caused differences in PBF only in the injured lung for each ROI compared with the control group (fig. 5).

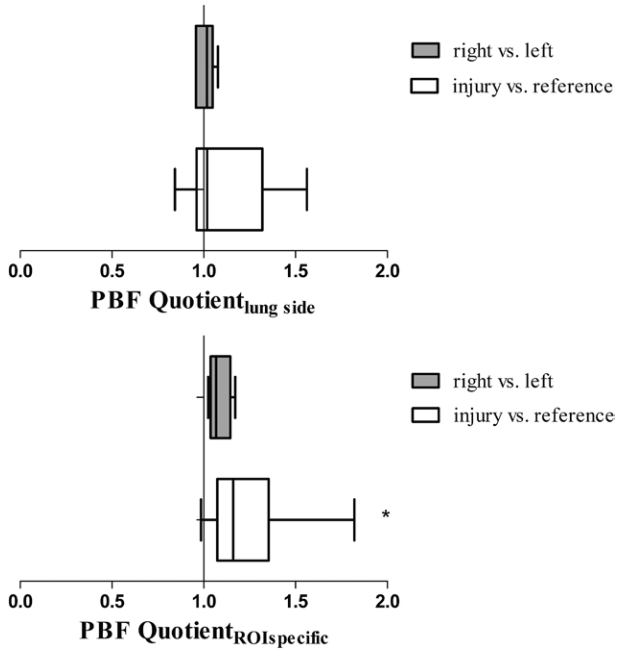

Fig. 3. Pulmonary blood flow (PBF) ratio of right/left side for the control group and injury/reference side for the entire lung (ROIlung side) and for a spherical region of interest of 0.24 cm^3 ($ROI_{specific}$). Higher mean concentrations of Ga-68 microspheres in the injured region yield a PBF quotient >1 in ROIlung side or $ROI_{specific}$. *$P < 0.0001$ compared with the control group. ROI = region of interest.

Local Density and PBF

PBF emission scans reconstructed with transmission scans obtained either before or after emission scans (see figure, Supplemental Digital Content 1, http://links.lww.com/ALN/A961) confirmed that temporal changes in lung density did not influence the detection of blood flow effects. Absolute differences in percent increase of PBF between the injured and the uninjured lung resulted in 1.2–3.3 (2.0 [1.4; 2.6]) (see table, Supplemental Digital Content 2, http://links.lww.com/ALN/A962).

Reconstruction of the PET image by using the transmission scan before the emission resulted in a PBF difference (injured and uninjured lung) of 19.3% [10.5; 28.8], whereas the calculation based on the transmission scan after emission resulted in a 19.7% [12.4; 29.3] difference. The absolute difference (2%) is much smaller than the increase in PBF difference (19.3%, 19.7%; $P < 0.001$), thus representing 10% of the measured PBF increase of the injured lobe.

Density Changes

All rats displayed a relatively larger imaged right lung volume (2.6 cm^3 [2.3; 3.8]) compared with left lung volume (2.0 cm^3 [1.7; 2.4]; $P = 0.02$). After aspiration, changes in density varied interindividually in size and magnitude and were observed exclusively in the middle and basal regions. Compared with the baseline CT scan, there were areas of

Table 2. Regional Pulmonary Blood Flow

	PBF		
	Control Group (n = 6)	Group Aspiration Left (n = 6)	Group Aspiration Right (n = 6)
Right lung	0.22 (0.19, 0.25)	0.23 (0.19, 0.25)	**0.22** (0.20, 0.23)
	$P = 0.68$	$P = 0.03$	$P = 0.06$
Left lung	0.22 (0.19, 0.24)	**0.25** (0.20, 0.28)	0.20 (0.19, 0.22)
$ROI_{specific\ right}$	0.27 (0.26, 0.32)	0.29 (0.25, 0.31)	**0.33** (0.31, 0.34)
	$P = 0.03$	$P = 0.03$	$P = 0.03$
$ROI_{specific\ left}$	0.26 (0.24, 0.28)	**0.33** (0.28, 0.34)	0.25 (0.23, 0.27)

Regional PBF values for the injured and reference regions of the control animals and animals that sustained aspiration injuries. The data are listed as the median values (25th percentile and 75th percentile) of six animals from each group. Data representing the values of injured ROIs are highlighted in bold. *P* values were calculated for the comparison of ROIs between the right and left lungs in each group. PBF = pulmonary blood flow; ROI = region of interest; $ROI_{specific}$ = spherical ROI of 0.24 cm^3 over the area with the greatest Ga-68 microsphere concentration on one side or is an identical ROI of the same volume over the anatomically corresponding area on the contralateral lung; $ROI_{specific}$ right = $ROI_{specific}$ of the right lung; $ROI_{specific}$ left = $ROI_{specific}$ of the left lung.

increased density in the CT images after aspiration in both the left lung (n = 6; size: 1.00 cm^3 [0.65; 1.41]) and the right lung (n = 6; 1.18 cm^3 [0.94; 1.3]) that represented 59% [43; 79] of the left lung, 48% [36; 61] of the right lung, and 23% [17; 29] of the entire imaged lung.

Lung density on the injured side within the $ROI_{specific}$ was found to range from −100 to 12.95 Hounsfield Units in nonaerated areas.

The fraction of mean density ratio (injury/reference side of $ROI_{specific}$) was 1.3 [1.2; 1.5].

This demonstrates that the injury increased the density of studied lung region. The same region had also a higher PBF injured/uninjured ratio. However, the comparison of the PBF and density ratios showed that they did not correlate (Pearson *r*: 0.28; $P = 0.37$).

Histological Findings

The DAD score values were slightly increased for the middle and basal ROIs (see figure, Supplemental Digital Content 3, http://links.lww.com/ALN/A963). The cumulative DAD scores were different in the basal ROI (fig. 6).

We found microspheres throughout the pulmonary vascular bed, even in acid-affected regions (fig. 7). Comparing microsphere numbers in the injured and the uninjured sides of the lung, we counted 15 [9; 17] and 14 [11; 23] microspheres for the apical layer, 27 [15; 35] and 16 [9; 27] microspheres for the middle layer, and 21 [17; 29] and 11 [10; 20] microspheres for the basal layer. These findings did not reach statistical significance.

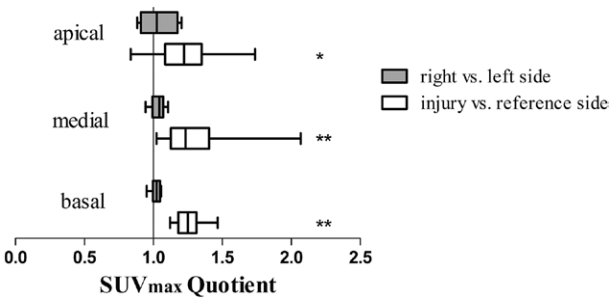

Fig. 4. Maximal standardized uptake value (SUV_{max}) ratio for the apical, medial, and basal region of interests, expressed as the quotient of SUV_{max} medians right/left side for the control group (n = 6) and SUV_{max} medians injured/reference (uninjured) side for all animals in the injury group (n = 12). Data are shown as the median values (25th and 75th percentile). *Statistically significant difference from the control group within the region of interest, at $P < 0.05$. **$P < 0.01$.

Discussion

Using the standardized acid aspiration model, we have shown effects of ALI on PBF in anesthetized, spontaneously breathing rats using small animal imaging techniques.

Our findings indicate that injured regions demonstrate increased PBF 10 min after acid aspiration and increased density in association with impairments in physiological variables within 50 min after injury.

Limitations of the Study

Although the acid aspiration technique has been standardized, the distally administered HCl may have been distributed unevenly. The amount of HCl delivered was limited to avoid dissemination to the contralateral lung. It remains unclear how well this model imitates aspiration injury in humans due to the absence of particulates, bacterial products, and cytokines.[17]

Critique of the PET technique used here has been previously discussed.[15] The data acquisition time for the PET scan was adjusted to obtain an optimal activity count rate. Changes in lung density during observation did not significantly influence the measured PBF derived from the volume data, which were reconstructed with attenuation correction using transmission scans before the emission scan. A caveat was our inability to assess CT scans concurrently with the PET scans. Another limitation was that the histological specimens could only be collected after the CT scan (50 min

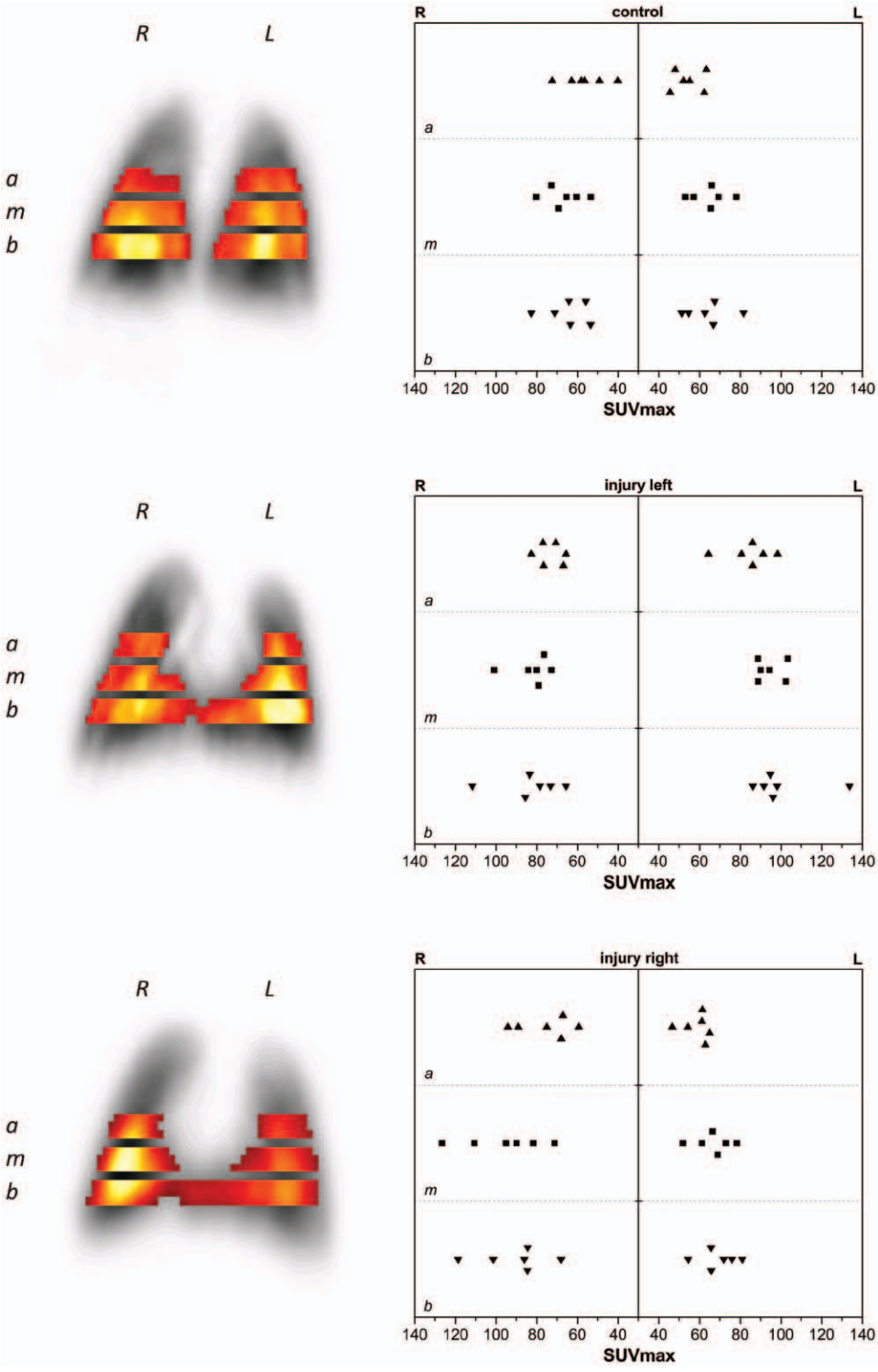

Fig. 5. Topographic distribution of pulmonary regional maximal standardized uptake value (SUV_{max}; g/ml) in three transverse regions of interest of equal height from the three groups (injury right group, injury left group, and control group) and for each lung side. *Triangles* and *rectangles* represent the individual median regional SUV_{max} for each animal. Positron emission tomography images in the coronal plane from three different animals (representing each group) illustrate the six region of interests that were used for the SUV_{max} calculation. Positron emission tomography–derived Ga-68 microsphere concentrations within the masks were color coded from relatively high (*white*) to low (*black*) and were normalized to the maximum concentration within the entire lung volume of each individual rat. a = apical; b = basal; L = left lung; m = medial; R = right lung.

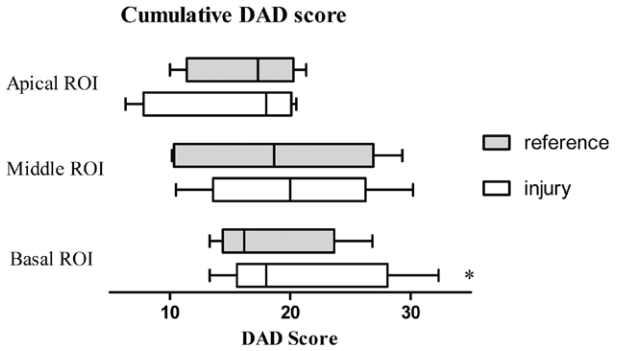

Fig. 6. The cumulative score for diffuse alveolar damage (DAD) demonstrates the sum of the averaged values for all presented features (alveolar edema, interstitial edema, microhemorrhage, inflammatory infiltration of polymorphonuclear neutrophils and macrophages, microatelectasis, and alveolar overdistension), including the apical, middle, and basal region of interest (ROI) after acid aspiration (n = 5) comparing injured and uninjured (reference) sides of these ROIs. Injured sides of the basal ROI demonstrate a higher cumulative DAD score value (P = 0.045).

after injury). However, the collected data represent a very early phase of pulmonary injury.

Acid Aspiration

Acid aspiration was performed as described in previous studies[7,12,13,17–20] in which the amount of instilled HCl varied (0.1–2 ml/kg). The amount of acid administered in the current study was in the lower range of effective doses, and this low volume is associated with a low mortality rate in rats.[21] By administering HCl directly *via* a tracheal tube, aspiration injury can be controlled to affect only a certain part of the lung,[22] although severity is dependent on the pH and the amount of acid.[17] This model has a definite, rather than diffuse, point of origin, which enables the researcher to study localized areas of injury. The insertion of the instillation catheter to a maximum depth makes it likely that the damage does not extend to the other side of the lung and that it affects only the basal and middle regions.

Similar to the previous study, although acid aspiration induced hypoxemia and hypotension with acidosis, the heart rate remained unchanged.[13]

PBF

Most of the PBF/perfusion data that published regarding ALI or acute respiratory distress syndrome describe the regional blood flow distribution after lung injuries such as surfactant depletion,[23,24] smoke inhalation,[25] and oleic acid[26,27] or endotoxin treatment.[28,29] PBF and perfusion data collected after acid aspiration have rarely been published[30] and to our knowledge, no blood flow data are currently available that concern the early phase (after 10 min) of acid-induced lung injury.

Both the control and the injury groups showed comparable entire lung ROI ratios between lung sides. However,

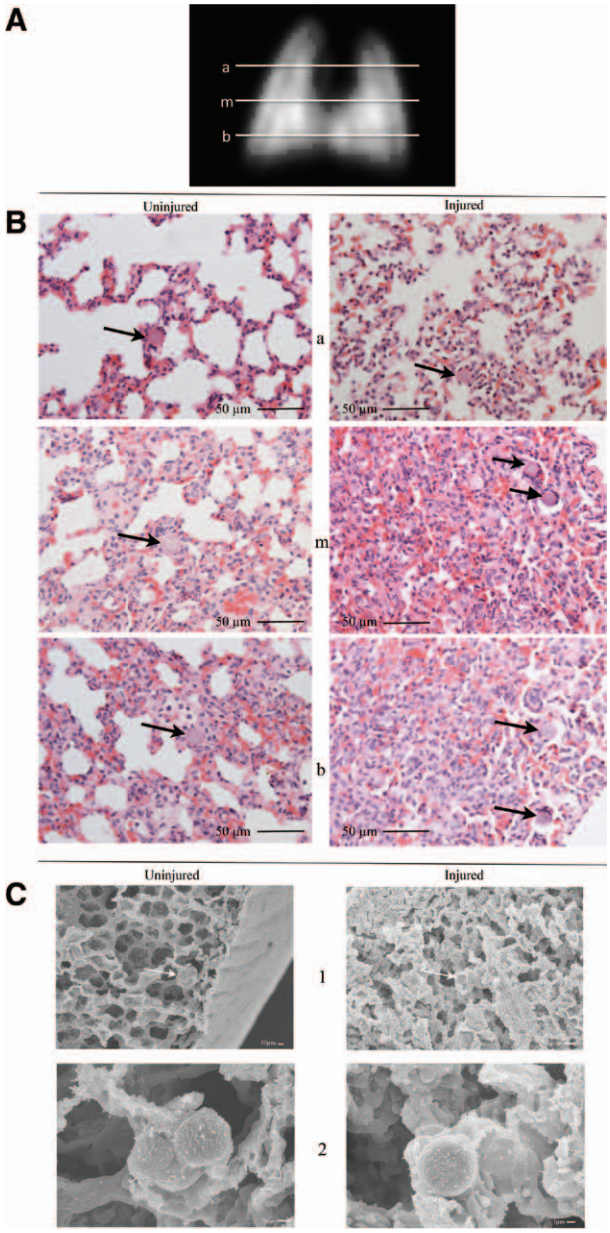

Fig. 7. Histological findings after the induction of acid aspiration. (*A*) Schematic representation of regions of interests where the specimens were removed (apical = a, medial = m, and basal = b). (*B*) Representative light microscopy photomicrographs of hematoxylin-eosin–stained sections of lung tissue from one animal after acid aspiration. Middle and basal regions of interests of the injured lung show areas with atelectasis and infiltrations compared with the reference (uninjured) lung. *Black arrows* indicate areas with microspheres surrounded by lung tissue. Original magnification: ×20; numeric aperture = 0.5. (*C*) Representative scanning electron microscopy image of basal sections of paraffin-embedded lung tissue from another animal, comparing the injured side with the uninjured reference side. *White arrows* indicate zones with microspheres (1), which are shown at greater magnification in (2). Microspheres were found inside the pulmonary vascular bed. The alveoli appeared irregular, and infiltration by neutrophils and macrophages was observed on the side of the injury, in contrast to the reference side. Original magnification: (1) ×300; (2) ×1,500.

the $ROI_{specific}$ ratios between the groups diverge due to the increased PBF in the injured area (fig. 3). The left and right lungs demonstrated equal PBF distributions in uninjured lungs. The increased PBF for the injured side in the left-lung injury group may reflect the smaller left lung volume leading to a larger, relative acid dose compared with the right-lung injury group. This phenomenon was not related to the magnitude of density changes revealed by the CT scans, and no differences were found between the sides with regard to their proportions of higher density tissue. Therefore, it can be assumed that factors, other than the size of injured tissue, such as the local concentration of HCl, may play a role in PBF distribution. Other parameters may include varying damaged functional structures. The difference in PBF distribution may also originate from the relatively small numbers of animals in each injury group.

Centered on areas of increased PBF after injury, $ROI_{specific}$ is associated with significantly increased PBF compared with the uninjured side. The increase in PBF within the region of injury also colocalized to regions of higher lung density in the CT scans. However, the PBF and CT values of the same region showed no correlation. This observation may be explained by the fact that the effect of the injury may not have extended throughout the entire ROI, which could have led to the underestimation of the calculated mean values. Another possibility is that the effect of the injury could have extended beyond the selected ROI, thus eluding detection. Because the PBF ratio varied from zero blood flow to maximal blood flow and the density in the same location varied from aerated to nonaerated, the maximal PBF in the injured region may have been accompanied by increases of varying magnitude in lung density. Increased maximal lung density may not predict maximal PBF (*i.e.*, due to edema formation with resulting extravascular pressure in the lung parenchyma).

The PBF on the injured side was higher than that of the control animals for all selected transversal planes (apical, medial, and basal). There was a difference between the right- and left-side injury groups. These observations suggest that the injuries affected the selected ROIs, although it is likely that the injuries to the left lung evoked an increase of the contralateral PBF. We were unable to explain this pattern by the larger involvement of morphological or functional structures. There was no evidence of varying left-lung damage levels, either in differences in lung density or in terms of gas exchange and circulation when comparing the left- and right-lung injured rats.

The distribution of PBF is dependent on oxygen tension,[31] and hypoxia was shown to cause similar regional changes in flow distribution in dogs and pigs,[32–34] with a shift of blood flow to the upper lung regions. A study in rats demonstrated that previous high-flow areas were hyperperfused during hypoxic exercise.[35] This type of hyperperfusion may have also occurred during local hypoxia in our study, resulting from blunted hypoxic pulmonary vasoconstriction after ALI.[36] During hypoxia, the endothelium releases relaxing factors that limit vasoconstriction in the pulmonary vascular bed.[37] Acid aspiration promotes local hypoxia and may attenuate hypoxic pulmonary vasoconstriction in injured regions, a finding also observed in sheep with pneumonia.[38] Hyperperfusion alone was shown not to be responsible for increased lung endothelial barrier protein permeability in sheep.[39] In contrast, hyperperfusion was associated with alveolar damage after single-lung ventilation in pigs.[40] The increased blood flow in areas of acid aspiration could intensify a loss of fluid through the damaged endothelium with subsequent local edema formation during the early stages of inflammation.

Density Changes

In a CT scan, an ideal method to assess lung damage,[41] the impact of acid on lung tissue is represented by an increase in tissue density in the injured areas.[13,42,43] We considered the influence of microspheres on CT lung density to be negligible due to the human albumin structure of the particles. In our study, the regions of increased density within the right- and left-side injury groups varied but did not differ substantially. The involved tissue extended over nearly one fourth of the total lung and approximately one half of the injured lung. These injury dimensions had a notable impact on gas exchange and circulation.

Acid Aspiration and Morphological Damage

Acid instillation creates a cellular injury to the alveolar epithelium and capillary endothelium,[17] which has been characterized as the increased production of basement membrane components, increased numbers of intraalveolar erythrocytes, the recruitment of neutrophils, and fibrin formation within 4 h of injury.[18] The cumulative DAD score showed no differences between apical regions but increased values for the lower ROIs of the injured side (fig. 6). Within the first hour after acid aspiration, histological abnormalities were localized to the areas of injury, and the differences observed with respect to the contralateral side were the result of inflammatory infiltration of neutrophils. Microatelectasis did not contribute to the cumulative increased DAD scores in basal regions (see figure, Supplemental Digital Content 3, http://links.lww.com/ALN/A963).

The histological investigations excluded the possibility of microsphere dropout from the alveolar capillaries. The samples did not demonstrate any accumulated microspheres due to microatelectasis or atelectasis, which implies that the PBF increases measured in this study were not the result of the consolidation of lung tissue.

Conclusion

The regional response of the lung to acid aspiration involves increased blood flow to the areas of injury and the deterioration of gas exchange during the early stages of the

inflammatory response. The results of our study suggest that early treatments administered *via* the blood stream have the potential to reach injured lung regions effectively. This type of experimental approach may contribute to the development of further treatment strategies that could be applied promptly after lung aspiration.

The authors thank Regina Herrlich, Technician, for assistance with animal preparation and Jörg van den Hoff, Ph.D., Professor, both from the Institute of Radiopharmacy, Helmholtz-Zentrum Dresden-Rossendorf, Dresden, Germany; and Jonathan Yaqub, Medical Student, Technische Universität Dresden, Faculty of Medicine Carl Gustav Carus, Dresden, Germany, and Guido Musch, M.D., Associate Professor of Anesthesia, Department of Anesthesia, Critical Care, and Pain Medicine, Massachusetts General Hospital and Harvard Medical School, Boston, Massachusetts, for their insightful comments.

References

1. Marik PE: Aspiration pneumonitis and aspiration pneumonia. N Engl J Med 2001; 344:665–71
2. Ware LB, Matthay MA: The acute respiratory distress syndrome. N Engl J Med 2000; 342:1334–49
3. Ferguson ND, Frutos-Vivar F, Esteban A, Gordo F, Honrubia T, Peñuelas O, Algora A, García G, Bustos A, Rodríguez I: Clinical risk conditions for acute lung injury in the intensive care unit and hospital ward: A prospective observational study. Crit Care 2007; 11:R96
4. Gajic O, Dabbagh O, Park PK, Adesanya A, Chang SY, Hou P, Anderson H III, Hoth JJ, Mikkelsen ME, Gentile NT, Gong MN, Talmor D, Bajwa E, Watkins TR, Festic E, Yilmaz M, Iscimen R, Kaufman DA, Esper AM, Sadikot R, Douglas I, Sevransky J, Malinchoc M; U.S. Critical Illness and Injury Trials Group: Lung Injury Prevention Study Investigators (USCIITG-LIPS): Early identification of patients at risk of acute lung injury: Evaluation of lung injury prediction score in a multicenter cohort study. Am J Respir Crit Care Med 2011; 183:462–70
5. Knight PR, Davidson BA, Nader ND, Helinski JD, Marschke CJ, Russo TA, Hutson AD, Notter RH, Holm BA: Progressive, severe lung injury secondary to the interaction of insults in gastric aspiration. Exp Lung Res 2004; 30:535–57
6. Rubenfeld GD, Caldwell E, Peabody E, Weaver J, Martin DP, Neff M, Stern EJ, Hudson LD: Incidence and outcomes of acute lung injury. N Engl J Med 2005; 353:1685–93
7. Safdar Z, Yiming M, Grunig G, Bhattacharya J: Inhibition of acid-induced lung injury by hyperosmolar sucrose in rats. Am J Respir Crit Care Med 2005; 172:1002–7
8. Bdeir K, Higazi AA, Kulikovskaya I, Christofidou-Solomidou M, Vinogradov SA, Allen TC, Idell S, Linzmeier R, Ganz T, Cines DB: Neutrophil alpha-defensins cause lung injury by disrupting the capillary-epithelial barrier. Am J Respir Crit Care Med 2010; 181:935–46
9. Azoulay E, Attalah H, Yang K, Herigault S, Jouault H, Brun-Buisson C, Brochard L, Harf A, Schlemmer B, Delclaux C: Exacerbation with granulocyte colony-stimulating factor of prior acute lung injury during neutropenia recovery in rats. Crit Care Med 2003; 31:157–65
10. Goldman G, Welbourn R, Klausner JM, Kobzik L, Valeri CR, Shepro D, Hechtman HB: Leukocytes mediate acid aspiration-induced multiorgan edema. Surgery 1993; 114:13–20
11. Folkesson HG, Matthay MA, Hébert CA, Broaddus VC: Acid aspiration-induced lung injury in rabbits is mediated by interleukin-8-dependent mechanisms. J Clin Invest 1995; 96:107–16
12. Rabinovici R, Vernick J, Hillegas L, Neville LF: Hypertonic saline treatment of acid aspiration-induced lung injury. J Surg Res 1996; 60:176–80
13. Pawlik MT, Schreyer AG, Ittner KP, Selig C, Gruber M, Feuerbach S, Taeger K: Early treatment with pentoxifylline reduces lung injury induced by acid aspiration in rats. Chest 2005; 127:613–21
14. Richter T, Bergmann R, Knels L, Beloiartsev A, Pietzsch J, Ragaller M, van den Hoff J: Increased PBF in areas of lung injury 10 minutes after aspiration as measured by PET (abstract). Am J Respir Crit Care Med 2010; 181:A5514
15. Richter T, Bergmann R, Pietzsch J, Közle I, Hofheinz F, Schiller E, Ragaller M, van den Hoff J: Effects of posture on regional pulmonary blood flow in rats as measured by PET. J Appl Physiol 2010; 108:422–9
16. Spieth PM, Knels L, Kasper M, Domingues Quelhas A, Wiedemann B, Lupp A, Hübler M, Neto AG, Gianella Neto A, Koch T, Gama de Abreu M: Effects of vaporized perfluorohexane and partial liquid ventilation on regional distribution of alveolar damage in experimental lung injury. Intensive Care Med 2007; 33:308–14
17. Matute-Bello G, Frevert CW, Martin TR: Animal models of acute lung injury. Am J Physiol Lung Cell Mol Physiol 2008; 295:L379–99
18. Kennedy TP, Johnson KJ, Kunkel RG, Ward PA, Knight PR, Finch JS: Acute acid aspiration lung injury in the rat: Biphasic pathogenesis. Anesth Analg 1989; 69:87–2
19. Amigoni M, Bellani G, Scanziani M, Masson S, Bertoli E, Radaelli E, Patroniti N, Di Lelio A, Pesenti A, Latini R: Lung injury and recovery in a murine model of unilateral acid aspiration: Functional, biochemical, and morphologic characterization. Anesthesiology 2008; 108:1037–46
20. Roch A, Michelet P, Lambert D, Delliaux S, Saby C, Perrin G, Ghez O, Bregeon F, Thomas P, Carpentier JP, Papazian L, Auffray JP: Accuracy of the double indicator method for measurement of extravascular lung water depends on the type of acute lung injury. Crit Care Med 2004; 32:811–7
21. James CF, Modell JH, Gibbs CP, Kuck EJ, Ruiz BC: Pulmonary aspiration—Effects of volume and pH in the rat. Anesth Analg 1984; 63:665–8
22. Schreiber T, Hueter L, Gaser E, Schmidt B, Schwarzkopf K, Rek H, Karzai W: PEEP has beneficial effects on inflammation in the injured and no deleterious effects on the non-injured lung after unilateral lung acid instillation. Intensive Care Med 2006; 32:740–9
23. Spieth PM, Carvalho AR, Pelosi P, Hoehn C, Meissner C, Kasper M, Hübler M, von Neindorff M, Dassow C, Barrenschee M, Uhlig S, Koch T, de Abreu MG: Variable tidal volumes improve lung protective ventilation strategies in experimental lung injury. Am J Respir Crit Care Med 2009; 179:684–93
24. Richter T, Bellani G, Scott Harris R, Vidal Melo MF, Winkler T, Venegas JG, Musch G: Effect of prone position on regional shunt, aeration, and perfusion in experimental acute lung injury. Am J Respir Crit Care Med 2005; 172:480–7
25. Willey-Courand DB, Harris RS, Galletti GG, Hales CA, Fischman A, Venegas JG: Alterations in regional ventilation, perfusion, and shunt after smoke inhalation measured by PET. J Appl Physiol 2002; 93:1115–22
26. Neumann P, Wrigge H, Zinserling J, Hinz J, Maripuu E, Andersson LG, Putensen C, Hedenstierna G: Spontaneous breathing affects the spatial ventilation and perfusion distribution during mechanical ventilatory support. Crit Care Med 2005; 33:1090–5
27. Wiener CM, Kirk W, Albert RK: Prone position reverses gravitational distribution of perfusion in dog lungs with oleic acid-induced injury. J Appl Physiol 1990; 68:1386–92
28. Gerbino AJ, McKinney S, Glenny RW: Correlation between ventilation and perfusion determines VA/Q heterogeneity in endotoxemia. J Appl Physiol 2000; 88:1933–42
29. Fernandez-Bustamante A, Easley RB, Fuld M, Mulreany D, Hoffman EA, Simon BA: Regional aeration and perfusion distribution in a sheep model of endotoxemic acute lung injury

characterized by functional computed tomography imaging. Crit Care Med 2009; 37:2402–11

30. Carlile PV, Hagan SF, Gray BA: Perfusion distribution and lung thermal volume in canine hydrochloric acid aspiration. J Appl Physiol 1988; 65:750–9
31. Melsom MN, Flatebø T, Nicolaysen G: Hypoxia and hyperoxia both transiently affect distribution of pulmonary perfusion but not ventilation in awake sheep. Acta Physiol Scand 1999; 166:151–8
32. Hlastala MP, Lamm WJ, Karp A, Polissar NL, Starr IR, Glenny RW: Spatial distribution of hypoxic pulmonary vasoconstriction in the supine pig. J Appl Physiol 2004; 96:1589–99
33. Lamm WJ, Starr IR, Neradilek B, Polissar NL, Glenny RW, Hlastala MP: Hypoxic pulmonary vasoconstriction is heterogeneously distributed in the prone dog. Respir Physiol Neurobiol 2004; 144:281–94
34. Starr IR, Lamm WJ, Neradilek B, Polissar N, Glenny RW, Hlastala MP: Regional hypoxic pulmonary vasoconstriction in prone pigs. J Appl Physiol 2005; 99:363–70
35. Kuwahira I, Moue Y, Urano T, Kamiya U, Iwamoto T, Ishii M, Clancy RL, Gonzalez NC: Redistribution of pulmonary blood flow during hypoxic exercise. Int J Sports Med 2001; 22:393–9
36. Schuster DP, Anderson C, Kozlowski J, Lange N: Regional pulmonary perfusion in patients with acute pulmonary edema. J Nucl Med 2002; 43:863–70
37. Brashers VL, Peach MJ, Rose CE Jr: Augmentation of hypoxic pulmonary vasoconstriction in the isolated perfused rat lung by *in vitro* antagonists of endothelium-dependent relaxation. J Clin Invest 1988; 82:1495–502
38. Easley RB, Fuld MK, Fernandez-Bustamante A, Hoffman EA, Simon BA: Mechanism of hypoxemia in acute lung injury evaluated by multidetector-row CT. Acad Radiol 2006; 13:916–21
39. Landolt CC, Matthay MA, Albertine KH, Roos PJ, Wiener-Kronish JP, Staub NC: Overperfusion, hypoxia, and increased pressure cause only hydrostatic pulmonary edema in anesthetized sheep. Circ Res 1983; 52:335–41
40. Kozian A, Schilling T, Fredén F, Maripuu E, Röcken C, Strang C, Hachenberg T, Hedenstierna G: One-lung ventilation induces hyperperfusion and alveolar damage in the ventilated lung: An experimental study. Br J Anaesth 2008; 100:549–59
41. Rouby JJ, Puybasset L, Nieszkowska A, Lu Q: Acute respiratory distress syndrome: Lessons from computed tomography of the whole lung. Crit Care Med 2003; 31(4 suppl):S285–95
42. Lim YS, Chung MH, Park SH, Kim HY, Choi BG, Lim HW, Kim JA, Yoo WJ: Acute and repeated inhalation lung injury by 3-methoxybutyl chloroformate in rats: CT-pathologic correlation. Eur J Radiol 2007; 62:227–34
43. Vieira SR, Puybasset L, Richecoeur J, Lu Q, Cluzel P, Gusman PB, Coriat P, Rouby JJ: A lung computed tomographic assessment of positive end-expiratory pressure-induced lung overdistension. Am J Respir Crit Care Med 1998; 158(5 Pt 1):1571–7